Self-Propulsion Mechanism of Active Janus Particles in Near-Critical Binary Mixtures

Sela Samin[*] and René van Roij

Institute for Theoretical Physics, Center for Extreme Matter and Emergent Phenomena,
Utrecht University, Leuvenlaan 4, 3584 CE Utrecht, The Netherlands

Gold-capped Janus particles immersed in a near-critical binary mixture can be propelled using illumination. We employ a nonisothermal diffuse interface approach to investigate the self-propulsion mechanism of a single colloid. We attribute the motion to body forces at the edges of a micronsized droplet that nucleates around the particle. Thus, the often-used concept of a surface velocity cannot account for the self-propulsion. The particle's swimming velocity is related to the droplet shape and size, which is determined by a so-called critical isotherm. Two distinct swimming regimes exist, depending on whether the droplet partially or completely covers the particle. Interestingly, the dependence of the swimming velocity on temperature is nonmonotonic in both regimes.

The study of self-propelling synthetic colloids is an area of intense active research [1,2]. The out-of-equilibrium directed motion of these colloidal microswimmers is maintained by a constant energy input which originates from their own activity. The directed swimming, coupled to the particle's rotational diffusion, leads to a significant increase in the effective diffusion coefficient [3–6] and to complex collective behavior, such as dynamical phase separation [7–9], clustering [10–12], and autonomous pumping [13]. Optimization of the microswimmers' design is essential for realizing applications such as targeted cargo and drug delivery, parallel assembly, and scavenging of contaminants [1,14,15].

The design of synthetic swimmers requires an understanding of the underlying mechanisms for the self-propulsion, e.g., self-diffusiophoresis [3,16–20], self-induced electrophoretic flow [21,22], and self-thermophoresis [4,23]. In many realizations, the particle motion is attributed to a microscopically thin boundary layer adjacent to the solid-fluid interface, which interacts with a self-generated field, such as the electrical potential, solute concentration, and temperature. Body forces within this layer give rise to an apparent slip velocity at the surface [24] while the fluid outside the interfacial layer is considered force-free. Thus, the particle motion is completely determined by the slip velocity distribution on its surface [19,25]. However, this simple picture breaks down when the self-generated field extends to a region with a size similar to that of the particle. In this Letter we explore such a scenario of self-diffusiophoresis due to a local solvent demixing, leading to a complex swimming behavior arising from the coupling of the self-generated chemical potential gradients and the fluid motion.

We focus on a recently realized new class of swimmers consisting of Janus colloids immersed in a near-critical binary mixture. Local heating of the colloid surface and the ensuing solvent demixing propels these particles, which exhibit fascinating individual and collective behavior [5–7,26,27]. A similar system was studied by Araki and Fukai [28] but in their simulations heating is periodically applied to the whole mixture. In this work we study the self-propulsion mechanism of a locally heated Janus swimmer (illustrated in Fig. 1) and show that it is fundamentally different from motion driven by interfacial velocities. Rather, we find that the particle motion is linked to the flow at the edges of a stationary demixed droplet, also far from the particle surface, and that it depends strongly on the solvent and particle properties. The advective effects, which are known to affect swimming in self-diffusiophoresis [29,30], are ignored in Würger's recent study of a similar system [31].

We consider a micronsized spherical colloid with radius R immersed in an unbounded homogeneous near-critical binary mixture. Half of the particle is gold-capped and continuously heated by irradiation. Owing to the gold layer's thickness being much smaller than R and its high thermal conductivity, we consider the cap to form an infinitely thin isothermal layer [23] with a temperature $T_0 > T_\infty$, where T_∞ is the fluid's ambient temperature. Local demixing of the fluid occurs if the temperature
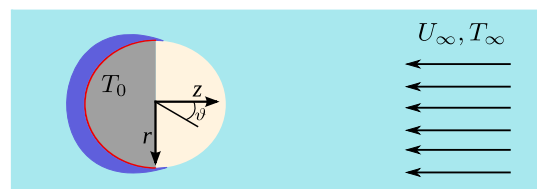

FIG. 1 (color online). Schematic illustration of a Janus particle immersed in a near-critical binary mixture at a temperature $T_\infty < T_c$. Illumination results in $T_0 > T_c$ at the gold-capped hemisphere (red line). At steady state, a demixed droplet is nucleated around the colloid translating at U_∞.

around the colloid increases above the (lower) critical temperature T_c of the mixture, of which both components are assumed to have a molecular volume a^3 with $a \sim 3$ Å. Consequently, temperature gradients in the demixed phase lead to gradients of the mixture chemical potential which give rise to a local body force. From azimuthal symmetry, no net torque will act on the colloid but since the temperature field is not spherically symmetric, the demixed droplet exerts a net force on the colloid in the axial direction. Hence, we set a cylindrical coordinate system in a frame of reference comoving with a colloid placed at its origin. Our aim is to find the axial velocity of the fluid far away from the colloid: $U_\infty = -U_\infty \hat{z}$ such that the colloid is force-free. The main result of this Letter is that the self-propulsion is a result of forces perpendicular to the colloid surface, and cannot be attributed to an effective surface velocity parallel to it, as is common in many scenarios [16,19,23,24].

We investigate the motion of the swimmer during the short-time ballistic regime of its enhanced diffusion trajectory [5,6]. A steady state is achieved quickly during the ballistic motion since the typical time scale for the phase-separation kinetics is much shorter than the particle rotational diffusion time [5,6]. We employ a well-established diffuse interface based approach [32], that couples the mixture order parameter $\varphi \in [-1/2, 1/2]$, the mixture chemical potential $k_B T \mu$, the fluid velocity $U_\infty v$, and the scaled temperature $\Theta = (T - T_\infty)/(T_0 - T_\infty)$ by the dimensionless equations

$$\partial \varphi / \partial t = -\nabla \cdot (\mathrm{Pe}_\varphi \varphi v - \nabla \mu), \tag{1}$$

$$\mu = -\epsilon \nabla^2 \varphi + f'(\varphi), \tag{2}$$

$$\nabla \cdot v = 0, \tag{3}$$

$$\nabla \cdot \tau = \nabla p + \mathrm{C}_h^{-1} \mathrm{Ca}^{-1} \varphi \nabla \mu, \tag{4}$$

$$\mathrm{Le}^{-1} \partial \Theta / \partial t = -\nabla \cdot (\mathrm{Pe}_T \Theta v - \nabla \Theta). \tag{5}$$

Here, all lengths are scaled by R and time is scaled by R^2/D, where D is the mixture interdiffusion constant.

Equation (1) is the convective Cahn-Hilliard equation governing the composition dynamics, where the relative magnitude of the composition advective flux, φv, and diffusive flux, $-D\nabla \mu$, is measured by the the composition Péclet number, $\mathrm{Pe}_\varphi = U_\infty R/D$. The chemical potential, Eq. (2), is obtained via the bulk free energy $f = (\chi - 2)\varphi^2 + 4\varphi^4/3$, where $\chi \sim 1/T$ is the Flory interaction parameter, supplemented by the square-gradient term which accounts for interfacial tension. The interfacial width is characterized by $\epsilon = \chi \mathrm{C}_h^2$, where $\mathrm{C}_h = a/R$ is the Cahn number. Equations (3) and (4) are the Stokes equations governing the fluid flow. Here, p and $\tau = \nabla v + \nabla v^T$ are the dimensionless fluid pressure and viscous stress

tensor, respectively, scaled by $\eta_f U_\infty / R$, where η_f is the fluid viscosity. The last term in Eq. (4), the body force due to gradients in the chemical potential, is proportional to the inverse capillary number, $\mathrm{Ca} = a^2 \eta_f U_\infty / k_B T$, which measures the relative magnitude of viscous and surface tension forces. Equation (5) is the energy equation for the fluid. Here, $\mathrm{Pe}_T = U_\infty R/\alpha$ is the thermal Péclet number, where $\alpha_f = k_f / (\rho_f C_f)$ is the fluid thermal diffusivity, and ρ_f, C_f, and k_f are the fluid density, heat capacity, and thermal conductivity, respectively. The Lewis number, $\mathrm{Le} = \alpha_f / D$, is the ratio of thermal to mass diffusivity.

The force, **F**, exerted on the colloid by the fluid is evaluated by applying the divergence theorem to Eq. (4):

$$\mathbf{F} = 2\pi \int_{-1}^{1} dc \, [p\mathbb{1} + \Pi - \tau] \cdot \mathbf{n}, \tag{6}$$

where $c = \cos \vartheta$, ϑ is the polar angle and $\mathbf{n}$ is the outward unit vector normal to the colloid surface. Equation (6) includes the contribution of the body force, which can be recast as $\nabla \cdot \Pi$ to obtain the Korteweg stress tensor [32], $\mathrm{C}_h \mathrm{Ca} \Pi = [\varphi f'(\varphi) - f - \frac{1}{2}\epsilon |\nabla \varphi|^2 - \epsilon \varphi \nabla^2 \varphi]\mathbb{1} + \epsilon \nabla \varphi \nabla \varphi$.

The physical properties are taken to best mimic the experimental setup in Ref. [6]. Therefore, we use properties of silica glass for the colloid and those of a critical water—2,6-lutidine for the fluid [33–36]. Since $T_0 - T_\infty$ is of the order of 1 K we assume that all material properties are constant; however, the assumption that D is constant is a somewhat crude approximation [36–38]. The exact value of the fluid-solid contact angle is unknown and we use the indicative values of $\theta_1 = \pi/4$ for the hydrophilic gold cap and set $\theta_2 = \pi/2$ for now.

Taking $R = 0.5$ μm, $D = 4 \times 10^{-11}$ m^2/s, and a large $U_\infty = 20$ μm/s leads to $\mathrm{Pe}_\varphi \approx 0.2$, $\mathrm{Pe}_T \approx 10^{-4}$, $\mathrm{Le} \approx 10^3$, $\mathrm{C}_h \approx 10^{-4}$ and $\mathrm{Ca} \approx 10^{-5}$. Even for this extremal U_∞, $\mathrm{Pe}_T \ll 1$ and we can safely neglect the heat advection in Eq. (5). In addition, because heat diffuses much faster than mass, $\mathrm{Le} \gg 1$, the temperature adjusts almost instantly to a composition perturbation and we may neglect also the time dependence in Eq. (5), which leads to the heat equation $\nabla^2 \Theta = 0$. The same argument holds for the solid and hence, the temperature distribution *only* depends on the thermal conductivity contrast of the solid and fluid, k_s / k_f, where k_s is the colloid conductivity. Therefore, we solve the heat equation once, and use the resulting temperature distribution as an input for the relaxation of the velocity and composition. This relaxation is dominated by the body force $\varphi \nabla \mu$ since $\mathrm{Ca} \ll 1$.

The colloid is placed at the origin of a cylindrical domain of height $z \in [-L, L]$ and radius $r \in [0, L]$ with $L = 500$. We use symmetry boundary conditions (BCs) at $r = 0$. At the other edges of the domain we impose a mixture of critical composition at a temperature T_∞ ($\Theta = 0$) with a velocity U_∞ [38]. At the cap we set the temperature $\Theta = 1$ while for the uncapped hemisphere we a have continuity of

the heat flux, $n \cdot k_f \nabla \Theta_{\mathrm{out}} = n \cdot k_s \nabla \Theta_{\mathrm{in}}$. In the diffuse-interface method, the no-slip BC for the velocity is imposed at the colloid surface: $v = 0$. The first BC for the composition on the colloid is no flux: $n \cdot \nabla \mu = 0$. The colloid has two chemically distinct solid-liquid interfaces, for which we assume an excess surface free energy F_w of the form $a^2 F_w / k_B T = \sum_i \int \gamma_i \varphi \, dA_i$, where $i = 1, 2$ denotes the capped and uncapped hemisphere, respectively, and γ_i measures the difference between the microscopic short-range interaction of the two solvent components and the solid. The wetting angles θ_i are then imposed using $n \cdot \nabla \varphi = -\tan{(\pi/2 - \theta_i)} |(\mathbb{1} - nn) \cdot \nabla \varphi|$, where in this so-called geometric formulation of the wetting BC $\gamma_i = \cos{\theta_i} / \sqrt{2}$ [39]. This BC has proved useful in simulations of moving contact lines where it is known to generate effective slip through the diffusive fluxes between the phases [39–41]. Thus, fluid motion at the colloid surface due to the short-range fluid-solid interaction is actually resolved even though the no-slip BC is imposed.

Steady state.—The resulting composition of the mixture around a force-free swimmer ($\mathbf{F} = 0$) for several T_∞ and fixed $T_0 = T_c + 0.5$ K is shown in Figs. 2(a)–2(d). The solid red line in each panel is the contour of the reduced critical temperature, $\Theta_c = (T_c - T_\infty)/(T_0 - T_\infty)$, which can account for many features of the swimming. Demixing only occurs inside the region bounded by the Θ_c isotherm, where $T > T_c$. In Fig. 2(a) we also show several other contours of $\Theta < \Theta_c$ (dashed lines). Demixing within these

FIG. 2 (color online). Steady state composition φ (right) and contours of the scaled pressure $p/200$ (left) around a heated Janus particle in the xOz plane. The temperature of the heated cap is $T_0 = T_c + 0.5$ K. The bulk mixture temperature approaches T_c from (a) to (d) with $T_c - T_\infty$ equal to (a) 2.75 K, (b) 1.5 K, (c) 1.1 K, and (d) 0.5 K. The red curve is the critical contour Θ_c. Arrows are vectors of the velocity (right) and body force [Eq. (4)] (left). The labels at the center of each panel indicate U_∞. In (a) the dashed lines are the contours $\Theta = 0.75, 0.69, 0.6, 0.5$. Here, $D = 4 \times 10^{-11}$ m²/s, $\theta_1 = \pi/4$ and $\theta_2 = \pi/2$.

contours will occur for fixed $T_0 > T_c$ and increasing T_∞ [see Figs. 2(b)–2(d)] or for fixed T_∞ and increasing T_0. In both cases Θ_c decreases and thus the droplet grows.

Figure 2 also reveals that a single water-rich ($\varphi > 0$) droplet is nucleated at the particle surface. Within the droplet the composition is inhomogeneous; φ is maximal at the surface and decays rather smoothly to the bulk value $\varphi = 0$ because of the temperature gradients and the proximity to T_c. The demixed region is clearly distinct from the bulk phase, as can be seen from the velocity vectors. Inside the demixed region the velocity is very small implying the droplet effectively moves together with the particle [42]. Strikingly, we find that no *significant* slip occurs near the solid-fluid interface, in contrast to the results in Ref. [31]. The fluid weakly circulates inside the droplet [38] and the overall flow pattern is similar to that of Stokes flow past a viscous droplet [43]. These observations hold even for the smallest droplet that allows for self-propulsion, which has a radial thickness of $\sim 0.1 R$.

We distinguish between two droplet shapes: (i) when $\Theta_c > \Theta_{\mathrm{cov}}$ the droplet partially covers the particle as in Figs. 2(a)–2(c) and (ii) for $\Theta_c < \Theta_{\mathrm{cov}}$ complete covering occurs as in Fig. 2(d). The covering temperature Θ_{cov} is closely related to the uncapped pole isotherm $\Theta_p = \Theta_c$, for which the demixed region should first encompass the particle. For the solid-fluid heat conductivity contrast $k_s/k_f \approx 3.5$ that we use, $\Theta_p \approx 0.7$. However, a thin demixed region at the pole is energetically costly, and in fact our numerical solution gives $\Theta_{\mathrm{cov}} \approx 0.66$ somewhat smaller than Θ_p and a discontinuity in the pole composition at Θ_{cov}. In comparison, for $k_s/k_f = 1$ the lower heat diffusivity in the solid leads to $\Theta_p = 0.5$ [23]. Hence, the droplet shape and therefore the swimming behavior are both quite sensitive to the conductivity contrast, which we thus identify as an interesting engineering parameter.

To maintain the steady-state shape of the droplet as dictated by the contour Θ_c, the composition diffusive flux $\propto \nabla \mu$ balances the convective flux according to Eq. (1). Therefore, the body force $\propto \varphi \nabla \mu$ is primarily large at the droplet diffuse boundary where advection becomes significant, see the vector maps in Fig. 2. Notice that the pressure contours in Fig. 2 are approximately perpendicular to $\varphi \nabla \mu$ because within the droplet $\nabla \cdot \tau$ is small, and thus $\nabla p \propto \varphi \nabla \mu$ to first order at steady state. Moreover, at the front of the droplet (with respect to the particle direction of motion) the diffusive flux must balance an advective flux toward the droplet whereas at the rear of the droplet the advective flux carries the mixture away from the droplet. Thus, also the body force at the droplet edge acts in opposite directions relative to the fluid flow, resulting in the pressure distributions of Figs. 2(a)–2(c) exhibiting two regions: (i) a $p > 0$ region at the droplet rear and (ii) a region of $p < 0$ near the three-phase contact line.

The extension of the body force far from the particle surface means there is no intrinsic separation of length
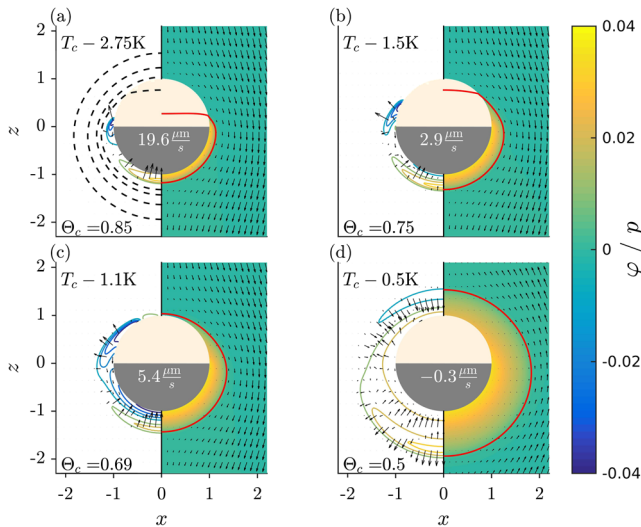
scales in the system and one cannot easily construct a force-free outer solution for the flow [24]. To describe the forces on the particle, one must account for the internal dynamics of the droplet, which cannot be reduced to the simple picture of a surface velocity. The anisotropy of the droplet shape produces an anisotropy also of the pressure and body force within the droplet, which is responsible for the particle motion. Thus, the self-propulsion is primarily a result of forces perpendicular to the surface, which are affected by the flow far from the surface, and cannot be mapped to an effective velocity on the colloid surface [44]. In Figs. 2(a)–2(c), the resulting force-free motion is in the direction of the uncapped hemisphere whereas the completely covered colloid in Fig. 2(d) moves with the capped hemisphere on the front.

Swimming velocity.—Figure 3 shows the swimming velocity U_∞ as a function of Θ_c for three values of the quenching $T_0 - T_c$, which increases with the laser intensity in experiments. U_∞ strongly depends on Θ_c and is of the order of 0.1–10 μm/s, in agreement with experiments. Two swimming regimes exist, for complete coverage at $\Theta_c < \Theta_{\mathrm{cov}}$ the swimming is independent of the quenching as Θ_c completely determines the demixed state. In contrast, for $\Theta_c > \Theta_{\mathrm{cov}}$ the curves are distinct with U_∞ increasing with quenching. This is because here Θ_c meets the particle surface at an angle different from the contact angle, which leads to a competition between the demixing and surface energies close to the three-phase contact line, with the balance shifted in favor of the demixing as quenching increases. Experiments are performed at a single constant T_∞, showing that the swimming velocity increases with the laser intensity [6], but our calculations, which explore a large range of T_∞, indicate this is not always the case.
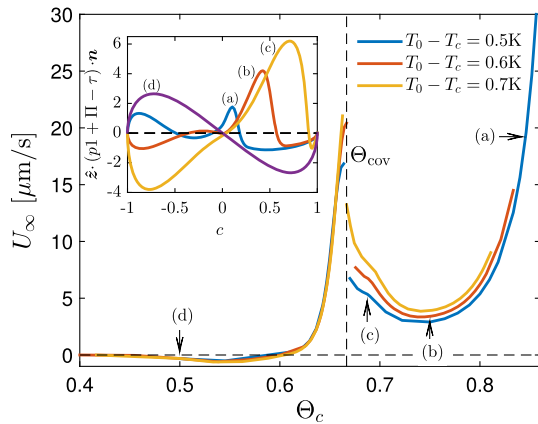

FIG. 3 (color online). Swimming velocity vs reduced critical temperature curves for three quenching temperatures $T_0 - T_c$. The droplet completely covers the colloid for $\Theta_c < \Theta_{\mathrm{cov}} \approx 0.66$ whereby the different curves collapse onto one another. For $\Theta_c > \Theta_{\mathrm{cov}}$ the curves are distinct with the swimming velocity increasing with quenching. The velocity of the swimmers in Fig. 2 is indicated with arrows and the inset shows the corresponding force profiles along the colloid contour.

Figure 3 also reveals that U_∞ jumps at Θ_{cov} and is nonmonotonic with Θ_c in both regimes. To understand this behavior we plot in the inset of Fig. 3 the z component of the force [cf. Eq. (6)] along the particle contour, $\hat{z} \cdot (p\mathbb{1} + \Pi - \tau) \cdot n$, as a function of c, where $c < 0$ ($c > 0$) corresponds the (un)capped hemisphere. The labels in the inset and the arrow labels in Fig. 3 correspond to the swimmers in the panels of Fig. 2. When Θ_c and U_∞ are large, as in Fig. 2(a), the force profile has a positive maximum in each hemisphere. This is because the droplet is small and hence a large body force exists close to the surface at both hemispheres. When Θ_c decreases and the droplet grows, as in Figs. 2(b)–2(c), the positive maximum at the capped hemisphere becomes a negative minimum while the maximum at the uncapped hemisphere grows in magnitude and moves to a larger c. This is a result of the anisotropic shape of the droplet. While the Θ_c contour is distanced from the capped hemisphere it remains close to the uncapped hemisphere and also covers a larger portion of it. Thus, the body force localized at the droplet edge becomes more significant near the three-phase contact line rather than near the particle rear, thereby accounting for the minimum in U_∞. For $\Theta_c < \Theta_{\mathrm{cov}}$, U_∞ first jumps to a larger positive value but then decreases with Θ_c since now the whole droplet boundary is distanced from the particle. U_∞ eventually becomes negative as the swimming direction reverses, see Fig. 2(d). This happens because the anisotropic temperature contours that completely circle the particle dictate that the droplet edge near the uncapped hemisphere is closer to the particle than at the capped hemisphere, leading to a larger pressure at the uncapped surface. Finally, U_∞ vanishes when Θ_c is small and the large droplet becomes quasispherical ($T_\infty \to T_c$).

The nucleation of a second, water-poor droplet, at the uncapped hemisphere is unfavored unless the hemisphere is very hydrophobic. The small volume of the demixed region around the uncapped hemisphere compared to the capped counterpart entails a relatively larger surface energy penalty. Nonetheless, we find that for $\theta_2 \gtrsim 0.8\pi$ a water-poor droplet does nucleate at the uncapped hemisphere. This is accompanied by a reversal of the swimming direction [38]. Assuming that the uncapped silica is hydrophilic [6,45], this result is consistent with the experimental observation that particles with a hydrophilic gold cap swim with their cap at the rear whereas for a hydrophobic cap it is at the front [6].

In conclusion, we have shown that a locally heated Janus particle in a near-critical binary mixture is propelled by the chemical potential gradients at the diffuse interface of a nucleated droplet, arising from the balance of diffusive and advective fluxes. Therefore, the self-propulsion cannot be described by an effective surface velocity. We hope that our results will stimulate further experiments to uncover the details of the swimming mechanisms of these intriguing particles and possibly explore other microswimmers propelled by nonlocal self-generated fields.

---

*S.Samin@uu.nl

[1] S. J. Ebbens and J. R. Howse, Soft Matter **6**, 726 (2010).
[2] I. S. Aranson, Phys. Usp. **56**, 79 (2013).
[3] J. R. Howse, R. A. L. Jones, A. J. Ryan, T. Gough, R. Vafabakhsh, and R. Golestanian, Phys. Rev. Lett. **99**, 048102 (2007).
[4] H.-R. Jiang, N. Yoshinaga, and M. Sano, Phys. Rev. Lett. **105**, 268302 (2010).
[5] G. Volpe, I. Buttinoni, D. Vogt, H.-J. Kummerer, and C. Bechinger, Soft Matter **7**, 8810 (2011).
[6] I. Buttinoni, G. Volpe, F. Kümmel, G. Volpe, and C. Bechinger, J. Phys. Condens. Matter **24**, 284129 (2012).
[7] I. Buttinoni, J. Bialké, F. Kümmel, H. Löwen, C. Bechinger, and T. Speck, Phys. Rev. Lett. **110**, 238301 (2013).
[8] J. Stenhammar, A. Tiribocchi, R. J. Allen, D. Marenduzzo, and M. E. Cates, Phys. Rev. Lett. **111**, 145702 (2013).
[9] T. Speck, J. Bialké, A. M. Menzel, and H. Löwen, Phys. Rev. Lett. **112**, 218304 (2014).
[10] I. Theurkauff, C. Cottin-Bizonne, J. Palacci, C. Ybert, and L. Bocquet, Phys. Rev. Lett. **108**, 268303 (2012).
[11] J. Palacci, S. Sacanna, A. P. Steinberg, D. J. Pine, and P. M. Chaikin, Science **339**, 936 (2013).
[12] O. Pohl and H. Stark, Phys. Rev. Lett. **112**, 238303 (2014).
[13] P. K. Ghosh, V. R. Misko, F. Marchesoni, and F. Nori, Phys. Rev. Lett. **110**, 268301 (2013).
[14] M. N. Popescu, M. Tasinkevych, and S. Dietrich, Europhys. Lett. **95**, 28004 (2011).
[15] L. Baraban, M. Tasinkevych, M. N. Popescu, S. Sanchez, S. Dietrich, and O. G. Schmidt, Soft Matter **8**, 48 (2012).
[16] R. Kapral, J. Chem. Phys. **138**, 020901 (2013).
[17] R. Golestanian, T. B. Liverpool, and A. Ajdari, Phys. Rev. Lett. **94**, 220801 (2005).
[18] U. M. Córdova-Figueroa and J. F. Brady, Phys. Rev. Lett. **100**, 158303 (2008).
[19] J. F. Brady, J. Fluid Mech. **667**, 216 (2011).
[20] J. de Graaf, G. Rempfer, and C. Holm, IEEE Trans. NanoBioscience **14**, 272 (2015).

[21] W. F. Paxton, K. C. Kistler, C. C. Olmeda, A. Sen, S. K. St. Angelo, Y. Cao, T. E. Mallouk, P. E. Lammert, and V. H. Crespi, J. Am. Chem. Soc. **126**, 13424 (2004).
[22] J. L. Moran and J. D. Posner, J. Fluid Mech. **680**, 31 (2011).
[23] T. Bickel, A. Majee, and A. Würger, Phys. Rev. E **88**, 012301 (2013).
[24] J. L. Anderson, Annu. Rev. Fluid Mech. **21**, 61 (1989).
[25] T. Bickel, G. Zecua, and A. Würger, Phys. Rev. E **89**, 050303 (2014).
[26] B. ten Hagen, F. Kümmel, R. Wittkowski, D. Takagi, H. Löwen, and C. Bechinger, Nat. Commun. **5**, 4829 (2014).
[27] F. Kümmel, B. ten Hagen, R. Wittkowski, I. Buttinoni, R. Eichhorn, G. Volpe, H. Löwen, and C. Bechinger, Phys. Rev. Lett. **110**, 198302 (2013).
[28] T. Araki and S. Fukai, Soft Matter **11**, 3470 (2015).
[29] S. Michelin and E. Lauga, J. Fluid Mech. **747**, 572 (2014).
[30] E. Yariv and S. Michelin, J. Fluid Mech. **768**, R1 (2015).
[31] A. Würger, preceding Letter, Phys. Rev. Lett. **115**, 188304 (2015).
[32] D. M. Anderson, G. B. McFadden, and A. A. Wheeler, Annu. Rev. Fluid Mech. **30**, 139 (1998).
[33] E. Gülari, A. F. Collings, R. L. Schmidt, and C. J. Pings, J. Chem. Phys. **56**, 6169 (1972).
[34] C. A. Grattoni, R. A. Dawe, C. Y. Seah, and J. D. Gray, J. Chem. Eng. Data **38**, 516 (1993).
[35] S. Pittois, G. P. Sinha, C. Glorieux, and J. Thoen, in *Thermal Conductivity 27/Thermal Expansion 15*, edited by H. Wang and W. Porter (DEStech Publications, Lancaster, 2004).
[36] S. Z. Mirzaev, R. Behrends, T. Heimburg, J. Haller, and U. Kaatze, J. Chem. Phys. **124**, 144517 (2006).
[37] K. Kawasaki, Ann. Phys. (N.Y.) **61**, 1 (1970).
[38] See Supplemental Material at http://link.aps.org/supplemental/10.1103/PhysRevLett.115.188305 for details.
[39] H. Ding and P. D. M. Spelt, Phys. Rev. E **75**, 046708 (2007).
[40] H.-Y. Chen, D. Jasnow, and J. Viñals, Phys. Rev. Lett. **85**, 1686 (2000).
[41] D. Jacqmin, J. Fluid Mech. **402**, 57 (2000).
[42] S. Yabunaka, R. Okamoto, and A. Onuki, Soft Matter **11**, 5738 (2015).
[43] C. Pozrikidis, *Introduction to Theoretical and Computational Fluid Dynamics* (Oxford University Press, USA, 2011).
[44] The mapping of the slip plane to the fluid-fluid interface is a natural alternative but is difficult in practice. The interface width is large due to the proximity to T_c such that the definition of a force-free domain is difficult and cannot be applied with simple criteria. It is of interest to explore if such a mapping is possible far from T_c.
[45] P. D. Gallagher and J. V. Maher, Phys. Rev. A **46**, 2012 (1992).